Rare Metal Materials and Engineering
Volume 55, Issue 6, June 2026
Available online at www.rmme.ac.cn

Science Press

Cite this article as: Yang Xiaoming, Liu Shengqiang, Huang Xiaomin, et al. Constitutive Model and Application of 2060 Aluminum-Lithium Alloy in Hot Stamping Process[J]. Rare Metal Materials and Engineering, 2026, 55(06): 1400-1408. DOI: https://doi.org/10.12442/j.issn.1002-185X.20250245.

ARTICLE

Constitutive Model and Application of 2060 Aluminum-Lithium Alloy in Hot Stamping Process

Yang Xiaoming[1], Liu Shengqiang[1], Huang Xiaomin[1], Ji Hongchao[1], Wang Baoyu[2,3]

[1] College of Mechanical Engineering, North China University of Science and Technology, Tangshan 063210, China; [2] School of Mechanical Engineering, University of Science and Technology Beijing, Beijing 100083, China; [3] Beijing Key Laboratory of Metal Lightweight Forming Manufacturing, Beijing 100083, China

Abstract: 2060 alloy, as the third generation aluminum-lithium (Al-Li) alloy, has lighter mass than traditional aluminum alloys and superior mechanical properties compared with previous generations of Al-Li alloy. The hot deformation behavior of 2060 Al-Li alloy sheets were investigated by hot tensile tests and model analysis. The fracture morphology was observed by scanning electron microscope. Then, the constitutive model coupled with the macroscopic mechanical behavior and the microstructure evolution was established. Finally, the established constitutive model was embedded in the finite element simulation software to analyze the deformation process of 2060 Al-Li alloy. The results show that the peak stress decreases with the increase in temperature and the decrease in strain rate. The deformation temperature has a significant impact on the anisotropy of the 2060 Al-Li alloy. It can be considered that the anisotropy can be eliminated at 400 °C or higher temperatures. It is found that the fracture process of 2060 Al-Li alloy conforms to typical ductile fracture laws. The presence of ridge improves the sheet deformation at elevated temperature. The constitutive model can predict the change of the true stress-true strain curves and the microstructure evolution accurately. The simulation results have good agreement with the experimental tests under hot stamping conditions.

Key words: constitutive model; 2060 Al-Li alloy sheet; hot stamping; anisotropy; FE simulation

1 Introduction

Compared with traditional high-strength aluminum alloys, the new generation of aluminum-lithium (Al-Li) alloys has great advantages, such as high specific strength, good corrosion resistance, and low density. Al-Li alloy has become one of the most promising lightweight materials in recent years due to its excellent physical and chemical properties. It is known as one of the most valuable lightweight alloy materials in the aviation industry of the 21st century[1]. Particularly, 2060 Al-Li alloy, which is the representative of third-generation Al-Li alloys, is used to manufacture the skin of the aircraft to supersede 7075 and 2024 Al alloys[2]. However, the Al-Li alloy sheet has low formability under the room temperature condition. It is not a good choice to produce the Al-Li alloy components at room temperature due to its poor plasticity. Raising the forming temperature of sheet is generally the best option to enhance formability for materials with low room-temperature plasticity[3]. Consequently, the hot stamping technique is used to produce the Al-Li alloy components.

The hot tensile deformation behavior serves as the foundation for researching the hot stamping formability of sheet. Therefore, it is crucial to study the high-temperature deformation behavior and fracture mode of sheet[4]. Studies show that heat treatment can modify the microstructure and mechanical characteristics as well as the subsequent deformation behavior[5]. Wang et al[6] studied the hot tensile behavior of 2195 Al-Li alloy sheet with different treatment states. It was found that the 2195-T8 Al-Li alloy exhibits a higher deformation activation energy and the best forming temperature is 475 – 500 ° C. However, the effect of heat treatment on the peak stress values can be ignored when the sheet is stretched at 400–500 °C. Consequently, an appropriate treatment state contributes to the investigation of thermal

Received date: June 08, 2025
Foundation item: The Youth Fund Project of Hebei Provincial Department of Education (QN2024242)
Corresponding author: Ji Hongchao, Ph. D., Professor, College of Mechanical Engineering, North China University of Science and Technology, Tangshan 063210, P. R. China, Tel: 0086-315-8805440, E-mail: jihongchao@ncst.edu.cn

deformation behavior of sheet. The hot deformation behavior of 2195-O Al-Li alloy were studied by Huang et al[7]. It is found that the plasticity of 2195-O Al-Li alloy increases with the increase in temperature and the decrease in strain rate when the deformation temperature is between 380 and 440 °C. Nevertheless, the tensile sample exhibits a poor elongation at 440 °C due to the coarse grains, which is lower than that at 380 °C. The deformation process of materials contains the influence of the external environment and the internal microstructure evolution. Tang et al[8] considered that the blocked dislocations and the damaged microstructure are caused by the deformation bands. Furthermore, an inappropriate range of deformation temperature and strain rate will lead to the precipitation of coarse T_1 phase in Al-Li alloy, resulting in uneven microstructure and affecting the macroscopic deformation behavior. Thus, the 2195-O Al-Li alloy has low workability at the temperature of 325–410 °C and strain rate of $10^{-2.5}$–10^{-3} s^{-1}.

There is a positive influence on the research of hot forming behavior by establishing the constitutive model. Yu et al[2] solved the relevant parameters of modified Arrhenius model for 2060 Al-Li alloy. Ge et al[9] developed a g-Johnson-Cook model for 2195 Al-Li alloy. This new model has a higher prediction accuracy compared with the Arrhenius model and Johnson-Cook model. The unified viscoplastic constitutive equation, as a constitutive model that can describe both macroscopic deformation and microstructural evolution of materials, has been widely used to describe the hot deformation behavior of aluminum alloys in recent years. Wang et al[10] proposed a unified viscoplastic constitutive model for 7075-O sheet under warm forming conditions. Yang et al[11] studied the hot deformation behavior of TC4 alloy by establishing the constitutive model. Zhou et al[12] studied the unified viscoplastic constitutive model of 22MnB5 at high temperature. According to the previous research, the unified viscoplastic constitutive model can be suitable for various isotropic materials to describe its stress-strain curves. Al-Li alloy exhibits strong anisotropic properties due to its special microstructure at room temperature. However, the anisotropy will be weakened with the increase in temperature[13]. It is crucial to study the hot deformation behavior by establishing the unified viscoplastic constitutive model for Al-Li alloy at a temperature range related to weak anisotropy or non-anisotropy.

The macroscopic fracture of sheet metal is mainly caused by the accumulation of microscopic damage[14], such as the grain, which has layered strain, has a high probability of crack deviation[15]. Feng et al[16] found that the coarse phase with high initial yield strength will induce the crack. Han et al[17] studied the effect of inhomogeneous microstructure on crack of 2050 Al-Li alloy. It was found that stress will concentrate at the edges of the corrosion grains, leading to damage. Jantarasricha et al[18] studied the fracture behavior of 2024 aluminum alloy sheet and established a damage model coupled into the finite element (FE) simulation software to predict the damage evolution. Xu et al[19] studied the anisotropic fracture of 7075 aluminum alloy sheet and proposed the fracture model to describe its damage. The crack form will change with the increase in temperature. It is helpful for analyzing the fracture behavior during the hot stamping process by studying the damage evolution process of Al-Li alloy at different temperatures. However, there is little research about the damage model of Al-Li alloy.

This work focused on the hot deformation and anisotropy behavior of the 2060 Al-Li alloy, and established a constitutive model coupled with microstructure evolution. Based on this, the hot tensile tests were conducted to study the stress-strain curves of 2060 Al-Li alloy at various temperatures and strain rates. The damage evolution process was observed by scanning electron microscope (SEM). Meanwhile, the anisotropic behavior of the alloy were studied at elevated temperatures. A unified viscoplastic constitutive model coupled with damage was established to predict stress-strain response and microstructure evolution. Finally, the established constitutive model was embedded in FE simulation model to verify the prediction accuracy of the model. A uniaxial hot tensile test and a hemispherical punch test were simulated using FE model coupled with constitutive equations.

2 Experiment

2.1 Materials

The Al-Li 2060-T8 alloy sheet with thickness of 2 mm was used as the research material in this study. The tensile strength and elongation are 530 MPa and 12%, respectively. The material has excellent mechanical properties under T8 condition. The chemical composition of the Al-Li alloy is displayed in Table 1. As the representative of the third-generation Al-Li alloys, the 2060 alloy has a lower content of element Li and a higher content of element Mg, compared with previous Al-Li alloys. Furthermore, multiple micro-alloying elements were added in the materials to improve the mechanical property.

2.2 Hot tensile test

The Gleeble-1500 thermal simulation experimental machine was used to study the hot deformation behavior of 2060 Al-Li alloy. The experimental device and temperature history of the sample are exhibited in Fig.1. A heating method with variable heating rate was adopted to prevent the sample overheating. The 2060 Al-Li alloy sheet was heated to 25 °C below the target temperature at a heating rate of 25 °C/s. And then, the heating rate was decreased to 5 °C/s until the sample temperature achieved the target deformation temperature. The sample were uniformly stretched to fracture after deformation at designed temperature for 180 s. Finally, the fractured samples were cooled by water. The tensile temperatures were 350, 400, and 450 °C, and the strain rates were 0.1, 1, and 5 s^{-1}.

Before the tests, the samples were immersed in the acetone solution to clean up the impurity on the surface. The tensile sample of 2060 Al-Li alloy is displayed in Fig.1b. The tensile

Table 1 Chemical composition of 2060 Al-Li alloy (wt%)

Li	Cu	Mg	Zn	Mn	Ag	Zr	Fe	Si	Al
0.80	3.60	0.80	0.35	0.30	0.33	0.11	0.02	0.01	Bal.

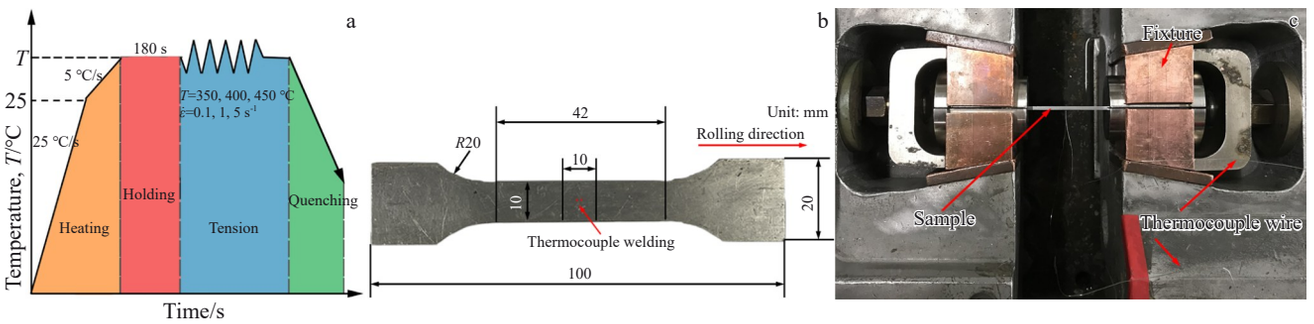

Fig.1 Schematic diagram of temperature history (a) and the appearances of tensile sample (b) and hot tensile machine (c)

direction is parallel to the rolling direction. Before the tests, the thermocouple wires were welded at the center of the sample to monitor the change of the temperature. Then, the sample was clamped on the hot tensile machine, as shown in Fig. 1c. After the experiments, the fracture samples were preserved to observe the fracture morphology.

3 Results

3.1 True stress-true strain curves

The true stress-true strain curves are shown in Fig. 2. The fracture strain increases with the increase in temperature. At strain rate of 5 s^{-1}, the fracture strain increases from 0.26 at 350 °C to 0.67 at 450 °C. It indicates that the plasticity of the 2060 Al-Li alloy can be significantly improved with the increase in deformation temperature. There is a positive correlation between the fracture strain and strain rate at 400 and 450 °C, while there is a negative correlation at 350 °C. It can be concluded that the formability of 2060 Al-Li alloy can be improved at high temperatures and high strain rates. The deformation temperature of this alloy is 400 °C at least, and the poor plasticity is achieved at 350 °C. The peak stress increases with the increase in strain rate, and decreases with increase in temperature.

Due to the extreme anisotropy of Al-Li alloy at room temperature, the anisotropy of 2060 Al-Li alloy was investigated in this study. The changes of stress at the loading direction of 0° and 45° were studied at the temperature of 350 and 400 °C. The results represent dramatic differences, as shown in Fig. 2d. The peak stress has large differences in the values between the loading direction of 0° and 45° at 350 °C. At 350 °C, the peak stress at the loading direction of 45° is 84.6 MPa, which is 15.01% less than that at the loading direction of 0° . It still exhibits significant anisotropy at 350 °C. However, the difference of stress is only 0.9 MPa between the loading direction of 0° and 45° when the deformation temperature increases to 400 °C. The anisotropy of 2060 Al-Li alloy disappears at 400 °C.

3.2 Fracture morphology

The fracture morphologies of the samples were observed by SEM after the hot tensile tests, as shown in Fig. 3. The material exhibits poor fracture morphology and shallow dimples at 350 °C. The poor fracture morphology indicates that 2060 Al-Li alloy exhibits low ductility when the deformation temperature is 350 °C or lower. The number of dimples gradually decreases with the increase in deformation temperature. However, the variation trend of dimple depth with deformation temperature is opposite to that of its quantity. It means that the material exhibits more obvious ductile fracture characteristics at higher temperatures. The fracture morphology has been significantly improved with the increase in deformation temperature. Meanwhile, more strengthening phases or inclusions are observed at high deformation temperature, as displayed in Fig.3b. Furthermore, the presence of ridge-like fracture interface surrounding the dimples is evident, indicating substantial plastic deformation prior to fracture in the 2060 Al-Li alloy. More strengthening phases and higher ridges are distributed in the fracture morphology at 400 and 450 °C, indicating great plasticity. Therefore, the 2060 Al-Li alloy can exhibit excellent plasticity and large fracture strain. This law aligns with the previously elucidated correlation between temperature and fracture strain.

According to the plastic damage theory, the process of plastic fracture in materials has three distinct stages: nucleation, growth, and aggregation of microvoids[20]. At elevated deformation temperatures, the nucleation rate of microvoids exhibits a decelerated pace, resulting in a reduction in their quantity. Consequently, there is an augmented proportion of microviods undergoing growth and aggregation, which gives rise to the emergence of larger microviods on the fracture surface, as depicted in Fig.3c.

4 Constitutive Model

4.1 Establishment of constitutive equations

There are two stages of elastic and plastic deformation during the large deformation process of the metal materials. The flow stress and elastic strain should follow the Hooke's law, and the equation can be expressed as follows:

$$\sigma = E\varepsilon_e = E\left(\varepsilon_T - \varepsilon_p\right) \quad (1)$$

where σ is the flow stress; ε_e, ε_T, and ε_p are the elastic strain, total strain, and the plastic strain, respectively; E is the Young's modulus, which is a temperature-dependent parameter.

The metal materials tend to exhibit significant viscoplastic behavior during deformation at high temperature. The flow stress is characterized by work hardening, viscous stress (σ_v),

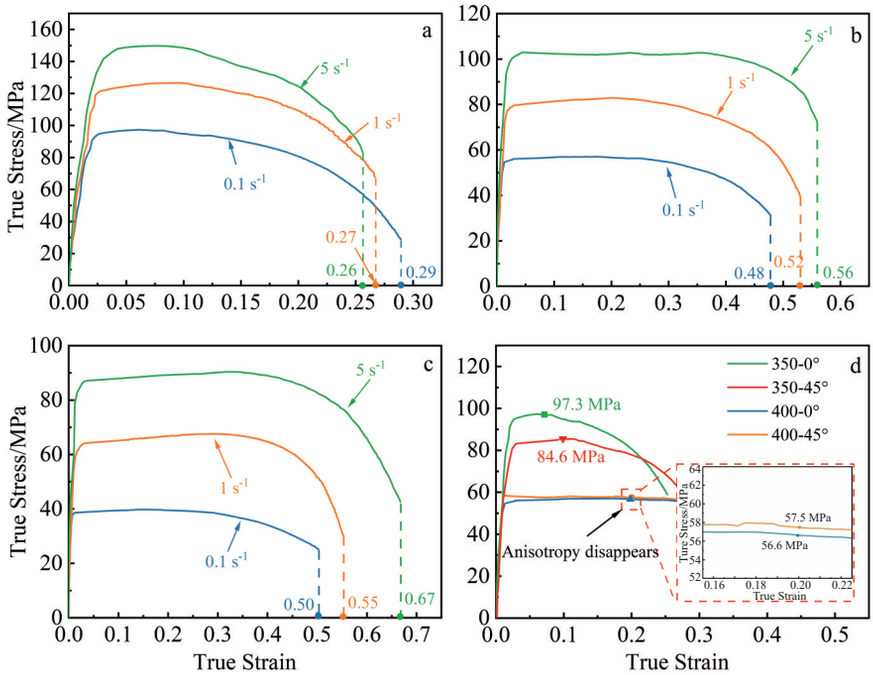

Fig.2 True stress-true strain curves of 2060 Al-Li alloy at different temperatures: (a) 350 °C, (b) 400 °C, and (c) 450 °C; true stress-true strain curves of 2060 Al-Li alloy along different tensile directions (d)

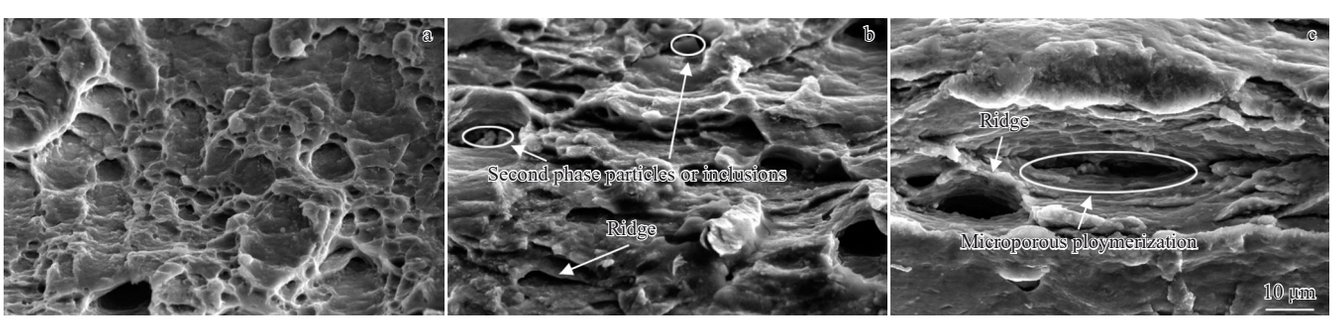

Fig.3 Fracture morphologies of 2060 Al-Li alloy at different temperatures and strain rate of 1 s^{-1}: (a) 350 °C, (b) 400 °C, and (c) 450 °C

and initial yield stress. It can be described as:

$$\sigma = k + H + \sigma_v \tag{2}$$

where H is the hardening stress, and k is the temperature-dependent initial yield stress.

The viscous stress is highly correlated with the strain rate, and their relationship can be expressed as:

$$\dot{\varepsilon}_p = \left(\frac{\sigma_v}{K}\right)^{n_1} = \left(\frac{\bar{\sigma} - H - k}{K}\right)^{n_1} \tag{3}$$

where $\bar{\sigma}$ is the equivalent stress, $\dot{\varepsilon}_p$ is the plastic strain rate, n_1 is the non-temperature-dependent material constant, and K is the temperature-dependent resistance coefficient.

Dislocation is a distinctive arrangement of atoms within a crystal lattice, forming a line defect characterized by elongation along a particular direction. Its presence exerts a profound influence on various physical and chemical properties, including crystal growth, phase transition, diffusion, deformation, and fracture. The microstructure evolution during high-temperature plastic deformation of metals relates to the alteration of dislocation density. Therefore, dislocation density serves as the internal variable for elucidating the isotropic hardening characteristics of materials in this constitutive model. However, the regularization of dislocation density was generally applied in engineering practice due to the extremely large order of magnitude of the dislocation density. The evolution of the dislocation density can be expressed as follows[21]:

$$\dot{\bar{\rho}} = A\left(1 - \bar{\rho}\right)\left|\dot{\varepsilon}_p\right| - C\bar{\rho}^{\delta} \tag{4}$$

where $\bar{\rho}$ is the regularization of dislocation density, which can be expressed as $\bar{\rho} = 1 - \rho_i/\rho$ with ρ_i as the initial dislocation density and ρ as the total dislocation density; δ is the material constant; A and C are the temperature-dependent parameters.

The growth of dislocations, dynamic recovery, and static recovery processes are taken into account in Eq.(4).

The stacking and interlacing of dislocations in materials will exhibit work hardening phenomenon at a macro level. Therefore, it is considered that the work hardening behavior of materials is a function related to dislocations. The equation about the hardening can be expresses as follows:

$$H = B\bar{\rho}^{0.5} \tag{5}$$

where B is a material constant related to temperature.

According to the abovementioned analysis, the anisotropy behavior of 2060 Al-Li alloy is distinct at 350 °C. However, the anisotropy of the studied alloy is eliminated at 400 °C or higher temperatures. Therefore, the 2060 Al-Li alloy is considered as the isotropic material, which follows the von Mises yield criterion when the temperature is higher than 400 °C. Meanwhile, the evolution of plastic damage is also isotropic. Based on this characteristic, this work focuses on the constitutive modeling and microstructure prediction of 2060 Al-Li alloy sheets at temperatures exceeding 400 °C.

In the field of continuous damage mechanics, it is commonly required to establish a damage variable that characterizes the progressive deterioration of a material resulting from the initiation, propagation, and merging of microvoids. The equation of damage evolution considering the plastic strain, plastic strain rate, and temperature can be expressed as[11]:

$$\dot{f}_{\mathrm{d}} = \frac{D_1 \dot{\varepsilon}_{\mathrm{p}}^{d_1}}{\left(1 - f_{\mathrm{d}}\right)^{d_2}} \sinh\left(D_2 \varepsilon_{\mathrm{p}}\right) \tag{6}$$

where $\dot{f}_{\mathrm{d}}$ is the damage change rate; f_{d} is the damage value; d_1, d_2, and D_2 are the material constants; D_1 is the temperature-dependent parameter.

After introducing the damage evolution, Eq. (1) and Eq. (3) can be written as Eq. (7) and Eq. (8), respectively.

$$\sigma = E\left(1 - f_{\mathrm{d}}\right)\left(\varepsilon_{\mathrm{T}} - \varepsilon_{\mathrm{p}}\right) \tag{7}$$

$$\dot{\varepsilon}_{\mathrm{p}} = \left[\frac{\sigma/\left(1 - f_{\mathrm{d}}\right) - R - k}{K}\right]^{n_1} \tag{8}$$

In summary, the unified viscoplastic constitutive model coupled with damage can be expressed as Eq. (9).

$$\begin{cases} \dot{\varepsilon}_{\mathrm{p}} = \left[\dfrac{\sigma/\left(1 - f_{\mathrm{d}}\right) - R - k}{K}\right]^{n_1} \\ H = B\bar{\rho}^{0.5} \\ \dot{\bar{\rho}} = A\left(1 - \bar{\rho}\right)\left|\dot{\varepsilon}_{\mathrm{p}}\right| - C\bar{\rho}^{\delta} \\ \dot{f}_{\mathrm{d}} = \dfrac{D_1 \dot{\varepsilon}_{\mathrm{p}}^{d_1}}{\left(1 - f_{\mathrm{d}}\right)^{d_2}} \sinh\left(D_2 \varepsilon_{\mathrm{p}}\right) \\ \sigma = E\left(1 - f_{\mathrm{d}}\right)\left(\varepsilon_{\mathrm{T}} - \varepsilon_{\mathrm{p}}\right) \end{cases} \tag{9}$$

The temperature-related parameters in Eq. (9) can be represented by Arrhenius equation[22], as shown in Eq.(10).

$$\begin{cases} K = K_0 \exp\left(Q_K / R_{\mathrm{g}} T\right) \\ E = E_0 \exp\left(Q_E / R_{\mathrm{g}} T\right) \\ C = C_0 \exp\left(Q_C / R_{\mathrm{g}} T\right) \\ k = k_0 \exp\left(Q_k / R_{\mathrm{g}} T\right) \\ B = B_0 \exp\left(Q_B / R_{\mathrm{g}} T\right) \\ D_1 = D_{10} \exp\left(Q_{D_1} / R_{\mathrm{g}} T\right) \end{cases} \tag{10}$$

where K_0, k_0, E_0, B_0, C_0, and D_{10} are the equation coefficients; T is the temperature; R_{g} is the gas constant of 8.31 J/(mol·K); and Q_K, Q_k, Q_E, Q_B, Q_C, and Q_{D_1} are the activation energy of materials.

4.2 Parametric solution

There are 16 material parameters in the established constitutive model. The parameter solving process mainly includes the following steps:

(1) The non-temperature-dependent material constant is solved by the experimental data, such as n_1.

(2) The temperature-dependent material constant is solved at different temperatures. The determined constants are fitted as temperature-dependent curves.

(3) The solved constants are used to solve the Arrhenius constant, which are shown in Eq. (10).

It is difficult to obtain correct results using conventional solving methods due to the highly coupled equations. Consequently, the genetic algorithm is conducted to solve the parameters in this study. The values obtained by above three steps are conducted as the initial values of the equation constants. The objective function is established to represent the similarity between model predicted values and experimental values, which can be written as follows[23–24]:

$$f(\boldsymbol{X}) = \frac{1}{M}\sum_{j=1}^{M}\left\{\frac{1}{N_j}\sum_{i=1}^{N_j} r_{ij}^2\right\} \tag{11}$$

where $\boldsymbol{X}$ is the vector of material constants that need to be optimized with $\boldsymbol{X}$=(x_1, x_2, ..., x_s); M is the number of true stress-true strain curves; N_j is the number of test data points obtained on the jth true stress-true strain curve; r_{ij} represents the square of the logarithm of the ratio between the calculated stress and the experimental stress.

The material parameters are optimized using the genetic algorithm, and the optimized results are shown in Table 2.

4.3 Results and accuracy evaluation

Fig. 4 shows the comparison results between the predicted

Table 2 Material constants optimized using the genetic algorithm

Parameter	Value
K_0/MPa	0.652
B_0/MPa	20.21
E_0/×10^3 MPa	4.5
Q_{k}/×10^2 J·mol^{-1}	3.512
Q_{C}/×10^3 J·mol^{-1}	1.823
A	8.0
n_2	1.1
d_1	0.901
D_2	0.1501
k_0/×10^{-2} MPa	2.21
C_0	101.1
Q_{K}/×10^4 J·mol^{-1}	2.602
Q_{B}/×10^3 J·mol^{-1}	5.577
Q_{E}/×10^3 J·mol^{-1}	1.5
n_1	10.1
D_{10}	0.4141
d_2	5.811
$Q_{\mathrm{D_1}}$/×10^4 J·mol^{-1}	1.614

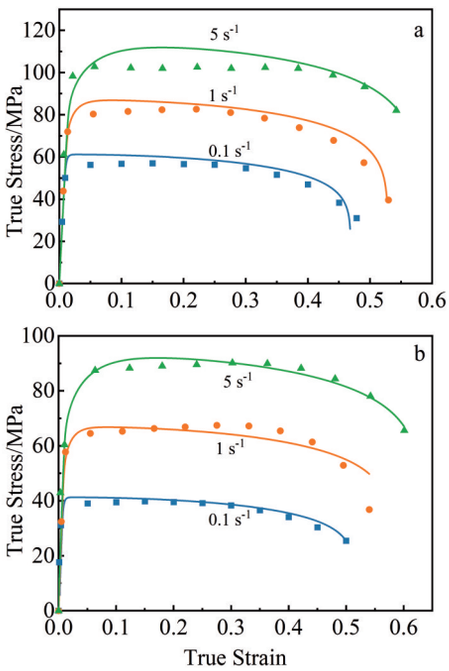

Fig.4 Comparison results between the model fitting curves and experimental values at different temperatures: (a) 400 °C; (b) 450 °C

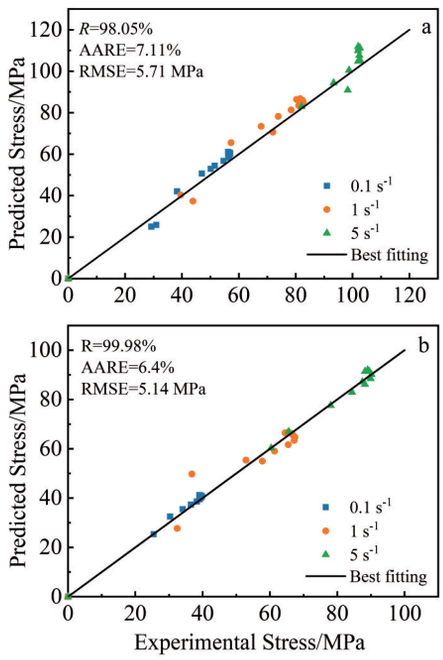

Fig.5 Correlation between the experimental and predicted stress values at different temperatures: (a) 400 °C; (b) 450 °C

values (solid curves) and experimental values (symbols) at different temperatures. The model-predicted results can accurately express that the curves rise by hardening and decline by the damage. Simultaneously, the effect of temperature and strain rate on the flow stress can also be described by the constitutive model. The predicted results have excellent agreement with the experimental values. Consequently, it can be concluded that the established constitutive model can predict the variations of the flow stress with great precision.

In order to accurately evaluate the predictive accuracy of the constitutive model, statistical evaluation indicators are adopted to describe the predictive ability of the model. The linear correlation coefficient (R), average absolute relative error (AARE), and root mean square error (RMSE) are used in this work, which can be expressed as follows[25]:

$$R = \frac{\sum_{i=1}^{N}\left(E_i - \bar{E}\right)\left(P_i - \bar{P}\right)}{\sqrt{\sum_{i=1}^{N}\left(E_i - \bar{E}\right)^2 \sum_{i=1}^{N}\left(P_i - \bar{P}\right)^2}} \tag{12}$$

$$\text{AARE} = \frac{1}{N}\sum_{i=1}^{N}\left|\frac{E_i - P_i}{E_i}\right| \tag{13}$$

$$\text{RMSE} = \sqrt{\frac{1}{N}\sum_{i=1}^{N}\left(E_i - P_i\right)^2} \tag{14}$$

where E_i and P_i are experimental data and predicted data, respectively; $\bar{E}$ and $\bar{P}$ are the mean values of experimental and predicted results, respectively; N is the number of the calculated points.

The correlation results at different temperatures are displayed in Fig. 5. The value of R exceeds 98% at the research temperatures. The maximum values of AARE and RMSE are 7.11% and 5.71 MPa, respectively. It can be found that the test data are distributed near the best fitting line, which indicates the great predictive accuracy.

According to the previous analysis, the decrease in flow stress curves of 2060 Al-Li alloy is mainly caused by the nucleation, growth, and coalescence of microvoids. Furthermore, the damage evolution is influenced by deformation temperatures and strain rates. The damage evolution behavior was investigated and predicted by the established constitutive model in this research. The change of the damage factor predicted by the model is shown in Fig. 6. All curves have the same trend under different conditions. The damage factor exhibits a gradual increasing trend when the level of deformation remains within a small range. This phenomenon is characterized by a slow rise in the damage factor, indicating that the microvoids are nucleating. The damage factor gradually increases over time as the deformation progresses. The rising rate of the damage factor also increases with the increase in strain, which indicates that the microvoids are growing. With the deformation progressing, the damage factor will increase rapidly. This phenomenon can be attributed to the cumulative effects and the coalescence of microvoids.

5 Application of Constitutive Model

5.1 FE simulation of hot tensile test

The established constitutive model of 2060 Al-Li alloy was embedded into the Abaqus software by the user subroutine. The hot tensile deformation process has been implemented in FE model, and the results of the strain distribution at 400 °C are shown in Fig. 7. It can be found that the maximum strain is mainly concentrated in the middle of

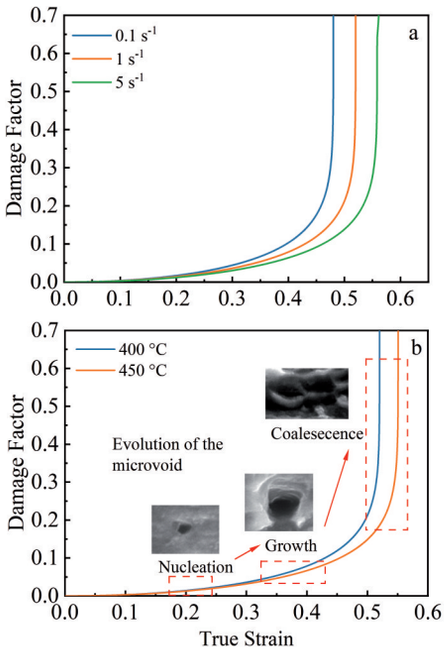

Fig.6 Changes of damage factor predicted by established constitutive model under different conditions: (a) 400 °C; (b) 1 s^{-1}

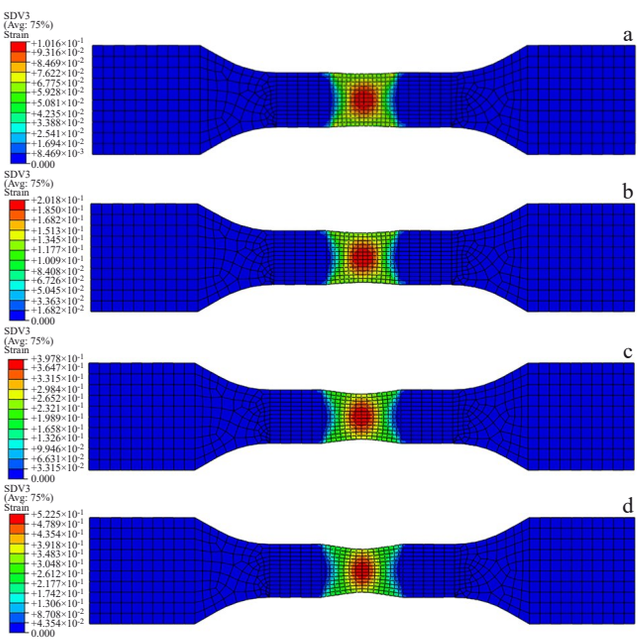

Fig.7 Strain distribution at different displacements: (a) 1.07 mm, (b) 2.2 mm, (c) 4.9 mm, and (d) 6.9 mm

the sample. The strain gradually decreases along the center to the end of the sample. Owing to the high temperature, the alloy at the center of the sample exhibits excellent plasticity and low resistance, thus undergoing significant deformation. The strain increases with the increase in displacement. The sample fractures when the tensile displacement reaches 6.9 mm, with a maximum strain of 0.52, which is consistent with the experimental results.

The damage factor distribution at 400 °C obtained by the simulation is displayed in Fig. 8. The damage is mainly concentrated at the center of the sample. There is significant necking appearing at the center of the sample with the increase in tensile displacement. The maximum damage location is the same as the maximum plastic strain location. The damage factor increases with the increase in displacement. The damage factor is 0.7021 when the displacement is 6.9 mm, which is considered that the sample is fractured. This is because the nucleation occurs at small deformations. With the increase in displacement, the number of crystal nuclei increases, and they gradually grow, eventually forming microvoids. It can be concluded that FE model combined with the established constitutive model can accurately predict the change of the damage and plastic strain.

5.2 FE simulation of hemispherical punch tests

FE model of hemispherical punch test has been conducted to analyze the formability of 2060 Al-Li alloy under hot stamping condition. In addition, the hemispherical punch stamping tests were conducted to measure the change of strain and thickness. The experimental tools and FE model are shown in Fig. 9. The tools contain die, holder, punch, heating wire, and so on. The punch was heated to the experimental temperature, which is same as the sheet temperature before the

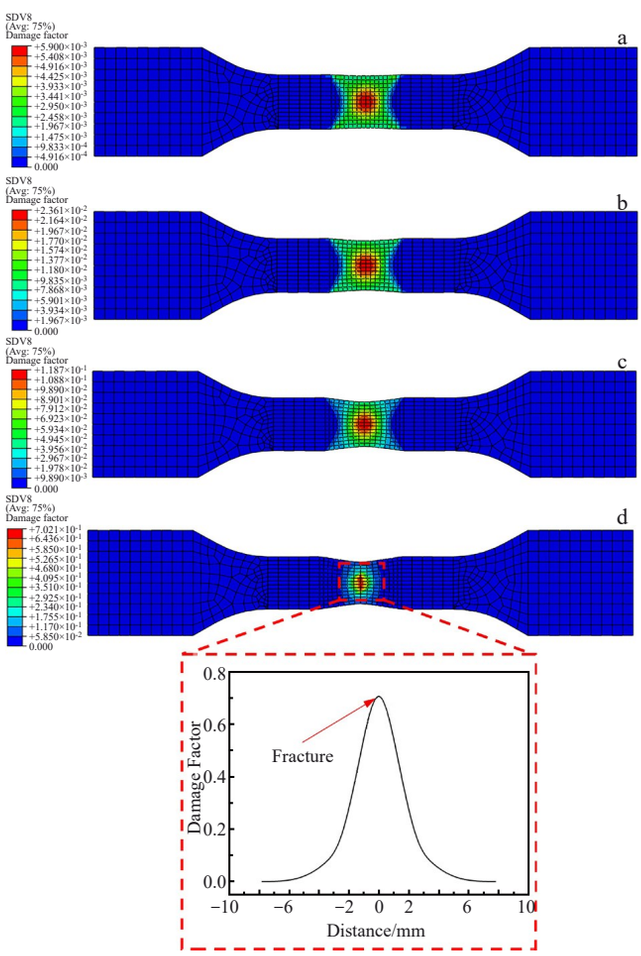

Fig.8 Damage factor distribution at different displacements: (a) 1.07 mm, (b) 2.2 mm, (c) 4.9 mm, and (d) 6.9 mm

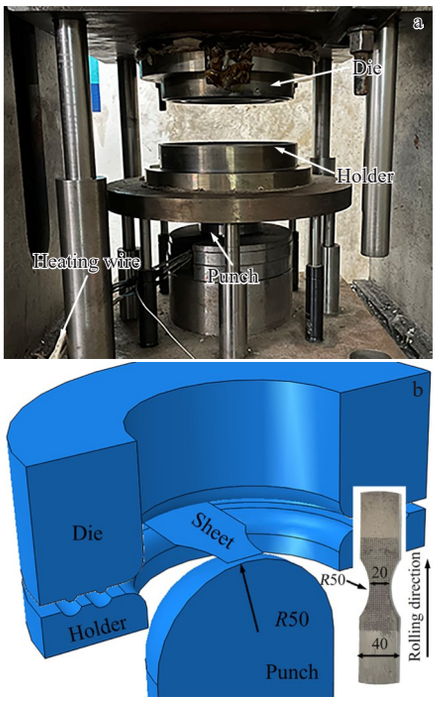

Fig.9 Photograph of experimental tools (a) and schematic diagram of FE model (b) of hemispherical punch stamping test

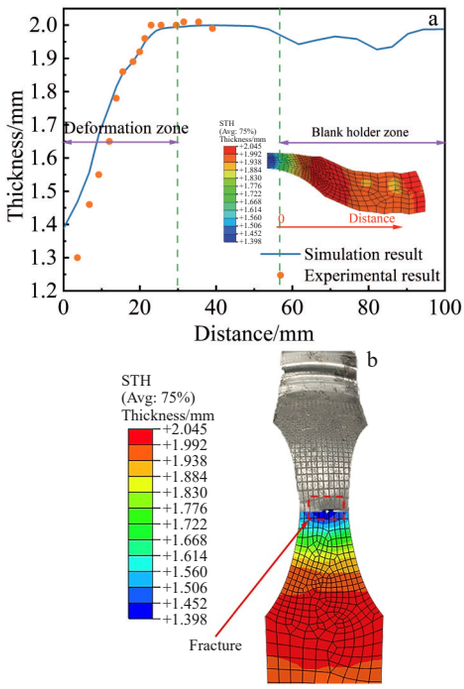

Fig.10 Comparison of thickness distribution between experiment and simulation results at 400 °C (a); distribution of sheet thickness at fracture (b)

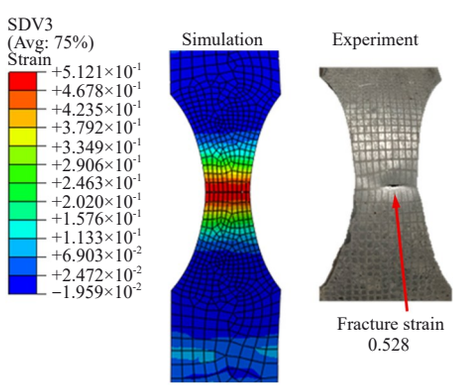

Fig.11 Strain distribution of the simulation and experiment results at 400 °C

tests. Therefore, the Al-Li alloy sheet can undergo deformation under the isothermal condition. The grooves with the depth of 3 mm were machined on the blank holder to eliminate the influence of insufficient holder force on the forming limit strain of the sheet during deformation. This feature is still set in FE model. The grids with the size of 2 mm×2 mm were etched on the surface of the sample to measure the change of strain, as shown in Fig. 9b. In FE model, the blank holder force was set as 10 kN to prevent the sheet sliding. In addition, the groove with a radius of 3 mm was machined in the holding area of the tools to eliminate the influence of sliding friction on formability. The sheet temperature and stamping speed were 400 °C and 40 mm/s, respectively. The radius of punch was 50 mm. The experimental process chose the same process parameters.

The distribution of sheet thickness is shown in Fig. 10. The thickness change has consistency between FE simulation results and experimental results. The minimum thickness appears at the center of the sheet according to the simulation result, which is 1.39 mm. The sheet thinning is restrained with the increase in distance. Similarly, necking and fracture occur at the center of the sheet, as shown in Fig.10b.

The strain distribution of the specimen at 400 °C is displayed in Fig. 11. The deformed grid was measured to calculate the sheet strain after tests. The maximum strain of the simulation and experiment results is 0.512 and 0.528, respectively. It can be concluded that FE model can predict the change of strain accurately. The mesh is elongated in the both simulation and experiment results.

6 Conclusions

1) The flow stress increases with the decrease in temperature and the increase in strain rate. The plasticity increases with the increase in strain rate at 400 and 450 °C. However, there is a negative correlation between plasticity and strain rate at 350 °C. In addition, the anisotropy is significant at 350 °C. It can be concluded that the formability of the 2060 Al-Li alloy is poor, which is not suitable for hot stamping at 350 °C. There is a good stamping performance at 400 and 450 °C.

2) According to the observation of fracture morphology, it is found that the 2060 Al-Li alloy exhibits a typical plastic fracture characteristic. The evolution of damage can be divided into three steps, including nucleation, growth, and

aggregation of microviods. The alloy exhibits poor fracture morphology and shallow dimples at 350 °C, which verifies the poor plasticity at microscopic perspective. More strengthening phases and higher ridges are distributed in the fracture morphology at 400 and 450 °C, indicating great plasticity.

3) The flow stress and microstructure evolution can be accurately predicted by the established constitutive model. Meanwhile, the strain and thickness distributions can be exactly simulated by the FE model embedded in the constitutive model. And the simulation results have good consistency with the experimental results.

References

1 Hu Tianjiao, Ye Lingying, Dong Yu *et al*. *Rare Metal Materials and Engineering*[J], 2023, 52(9): 3230 (in Chinese)

2 Yu Yibiao, Chen Leping, Xu Yong *et al*. *Rare Metal Materials and Engineering*[J], 2021, 50(12): 4388 (in Chinese)

3 Zhou J, Yang X M, Wang B Y *et al*. *The International Journal of Advanced Manufacturing Technology*[J], 2023, 127: 5293

4 Li Y, Xu G F, Guo G Y *et al*. *Materials Characterization*[J], 2023, 204: 113170

5 Wang Xiaobo, Rong Li, Huang Hui *et al*. *Rare Metal Materials and Engineering*[J], 2024, 53(1): 250 (in Chinese)

6 Wang Ruiqi, Dai Guoqing, Guo Yanhua *et al*. *Journal of Central South University*[J], 2023, 30(5): 1417

7 Huang X M, Guan B, Wang B Y *et al*. *Journal of Alloys and Compounds*[J], 2023, 946: 169426

8 Tang J G, Yi Y P, He H L *et al*. *Journal of Alloys and Compounds*[J], 2023, 934: 167755

9 Ge X Q, Yu J Q, Sun Y T *et al*. *Materials & Design*[J], 2024, 244: 113100

10 Wang Y, Liu K N, Hu N *et al*. *Engineering Fracture Mechanics*[J], 2020, 235: 107154

11 Yang X M, Wang B Y, Zhou J *et al*. *Archives of Civil and Mechanical Engineering*[J], 2021, 21: 69

12 Zhou J, Mu Y H, Wang B Y. *International Journal of Mechanical Sciences*[J], 2017, 133: 457

13 Ning J, Liang J K, Hu X Y *et al*. *Materials*[J], 2023, 16(14): 5012

14 Pandya K S, Roth C C, Mohr D. *International Journal of Plasticity*[J], 2020, 135: 102788

15 Esin V A, Francois M, Belkacemi L T *et al*. *Materials Science and Engineering A*[J], 2022, 858: 144120

16 Feng B, Gu B, Li S H. *Materials Science and Engineering A*[J], 2022, 848: 143396

17 Han C, Yu M, Jia X J *et al*. *Corrosion Science*[J], 2024, 235: 112213

18 Jantarasricha T, Chongbunwatana K, Panich S. *International Journal of Applied Mechanics*[J], 2023, 15(1): 2250093

19 Xu T Y, Li F G, Wang X L *et al*. *Journal of Engineering and Performance*[J], 2023, 32(7): 3230

20 Zhu Biwu, Xiao Gang, Liu Xiao *et al*. *Rare Metal Materials and Engineering*[J], 2025, 54(3): 722 (in Chinese)

21 Lin J G, Cao J, Balint D. *Microstructure Evolution in Metal Forming Processes*[M]. Cambridge: Woodhead Publishing Limited, 2012: 180

22 Su Z X, Sun C Y, Wang M J *et al*. *Journal of Magnesium and Alloys*[J], 2022, 10(1): 281

23 Cao J, Lin J G. *International Journal of Mechanical Sciences*[J], 2008, 50(2): 193

24 Lin J G, Yang J B. *International Journal of Plasticity*[J], 1995, 15(11): 1181

25 Chen Peng, Li Jinshan, Li Chongchong *et al*. *Rare Metal Materials and Engineering*[J], 2025, 54(6): 1613 (in Chinese)

2060铝锂合金热冲压成形本构模型及应用

杨晓明[1]，刘胜强[1]，黄晓敏[1]，纪宏超[1]，王宝雨[2,3]

(1. 华北理工大学 机械工程学院，河北 唐山 063210)

(2. 北京科技大学 机械工程学院，北京 100083)

(3. 北京市轻量化成形制造重点实验室，北京 100083)

摘　要：2060合金作为第三代铝锂合金，与传统铝合金相比质量更轻，与前几代铝锂合金相比机械性能更优越。通过热拉伸实验和模型分析研究了2060铝锂合金板材的热变形行为。通过扫描电子显微镜观察断裂形态，建立宏观力学行为和微观组织演变相结合的本构模型。最后，将建立的本构模型嵌入有限元模拟软件中，分析了2060铝锂合金的变形过程。结果表明，峰值应力随着温度的升高和应变速率的降低而降低，变形温度对2060铝锂合金的各向异性有显著影响；在400 ℃或更高的温度下可以消除板料各向异性；本构模型准确预测了真实应力-真实应变曲线的变化和微观结构的演变；通过断口形貌分析发现，2060铝锂合金断裂形式为典型的韧性断裂，断口处出现的峰脊促进了板料在高温下的变形。仿真结果与热冲压条件下的实验测试结果具有较好的一致性。

关键词：本构建模；2060铝锂合金板材；热冲压；各向异性；有限元仿真

作者简介：杨晓明，男，1993年生，博士，华北理工大学机械工程学院，河北 唐山 063210，电话：0315-8805440，E-mail：yangxm@ncst.edu.cn